

# All-in-One Transferring Image Compression from Human Perception to Multi-Machine Perception

Jiancheng Zhao  
The University of  
Tokyo  
Tokyo, Japan

Xiang Ji  
The University of  
Tokyo  
Tokyo, Japan

Zhuoxiao Li  
The University of  
Tokyo  
Tokyo, Japan

Zunian Wan  
The University of  
Tokyo  
Tokyo, Japan

Weihang Ran  
The University of  
Tokyo  
Tokyo, Japan

Mingze Ma  
The University of  
Tokyo  
Tokyo, Japan

Muyao Niu  
The University of  
Tokyo  
Tokyo, Japan

Yifan Zhan  
The University of  
Tokyo  
Tokyo, Japan

Cheng-Ching  
Tseng  
Peking University  
Beijing, China

Yinqiang Zheng\*  
The University of  
Tokyo  
Tokyo, Japan

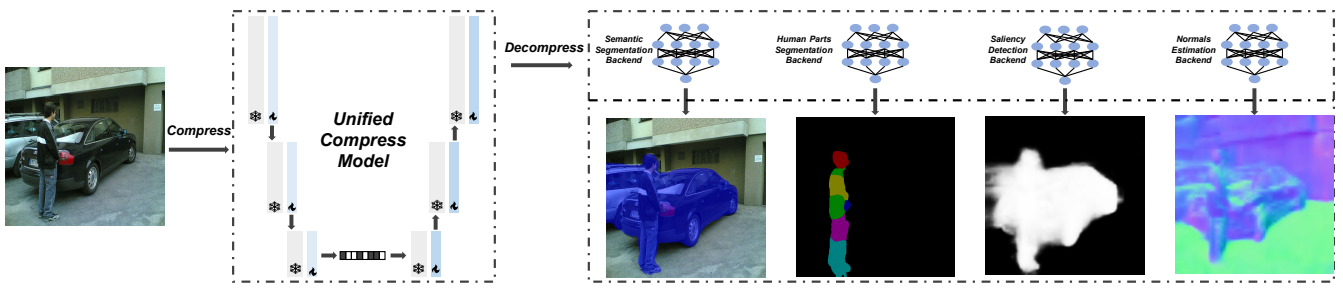


Figure 1: Our unified model leverages lightweight tuning modules (Gray: frozen base codec; Blue: tuning modules) to efficiently transfer a human-centric codec into a multiple machine vision codec, requiring only a single training and inference process.

## Abstract

Efficiently transferring Learned Image Compression (LIC) model from human perception to machine perception is an emerging challenge in *vision-centric representation learning*. Existing approaches typically adapt LIC to downstream tasks in a single-task manner, which is inefficient, lacks task interaction, and results in multiple task-specific bitstreams. To address these limitations, we propose an asymmetric adaptor framework that supports multi-task adaptation within a single model. Our method introduces a shared adaptor to learn general semantic features and task-specific adaptors to preserve task-level distinctions. With only lightweight plug-in modules and a frozen base codec, our method achieves strong performance across multiple tasks while maintaining compression efficiency. Experiments on the *PASCAL-Context* benchmark demonstrate that our method outperforms both Fully Fine-Tuned and other Parameter Efficient Fine-Tuned (PEFT) baselines, and validating the effectiveness of multi-vision transferring.

## CCS Concepts

- Computing methodologies → Artificial intelligence; Machine learning.

## Keywords

Image Compression, Machine Learning, PEFT

## 1 Introduction

Image coding for machine (ICM) has become increasingly important in recent years, driven by the fact that more and more visual data is processed by machines rather than viewed by humans. This trend is particularly pronounced with the growing dominance of large-scale vision-language model (VLM) training. The core objective of ICM is to learn compact visual representations that reduce transmission cost while preserving accuracy for downstream machine vision tasks. A straightforward solution is to customize the encoder, decoder, or bitstream in a task-specific manner [3, 7, 10, 15–17, 28, 29].

However, such task-specific customization often leads to expensive training, increased bitrate consumption, and substantial parameter overhead. Therefore, motivated by the observation that the most accessible base codecs—optimized for human perception—already produce high-quality reconstructions that preserve most of the semantic content in images, recent works propose to adapt them using parameter-efficient fine-tuning (PEFT) directly. By updating only a small number of parameters, these approaches aim to retain the original human-perception quality of the base codec, while efficiently transferring the latent features and the reconstructed images into a more semantically compact space that is better aligned with downstream machine vision tasks. Despite the efficiency advantages of PEFT-based adaptation, existing methods primarily focus on single-task transfer, treating each task in a completely independent and isolated manner, as shown in Table 1, which incurs several limitations: (1) Each task still requires

\*Corresponding author. Email address: yqzheng@ai.u-tokyo.ac.jp

**Table 1: Comparison of representative codec transfer methods in terms of parameter efficiency and multi-task transferability. A method is considered *Efficient* if it enables adaptation with only a small number of trainable parameters, and supports *Multi-Task Transfer* if it allows joint optimization across multiple downstream tasks.**

Method	Efficient	Multi-Task Transfer
Full-Finetune	✗	✗
ICMH-Net [29] (MM’23)	✓	✗
TransTIC [8] (ICCV’23)	✓	✗
AdaptICMH [24] (ECCV’24)	✓	✗
<b>Ours</b>	✓	✓

separately customized training, which is inefficient and hinders scalability as the number of tasks increases; (2) The lack of cross-task interaction prevents the model from learning shared representations across related task domains; (3) Independent adaptation leads to task-specific bitstreams, resulting in additional storage overhead and deployment complexity.

To address the limitations of existing single-task adaptation methods, we propose an asymmetric adaptor framework that enables efficient multi-task transfer within a unified image compression model, as shown in Figure 1. Specifically, to extract task-general and semantically compact features, we introduce a Shared Adaptor, inserted during the Analysis transform (Encoder) and shared across all tasks. This module captures common semantic patterns in a task-agnostic and parameter-efficient manner, serving as a global representation pool. To preserve task-specific information and prevent mutual interference, we introduce a Task Adaptor in the Synthesis transform (Decoder). Each Task Adaptor consists of parallel, task-specific branches that independently modulate features according to the needs of each downstream task. Both components are lightweight, plug-and-play, and trained via a parameter-efficient strategy, ensuring minimal overhead while preserving the base codec’s original compression performance. Together, these modules enable a balance between effective feature sharing and explicit task decoupling, supporting scalable and flexible multi-task adaptation.

Overall, our contributions are as follows:

- We propose an asymmetric adaptor framework for efficient multi-task adaptation of pre-trained image codecs, enabling a unified model to support multiple downstream tasks
- We design two lightweight plug-in modules—Shared Adaptor and Task Adaptor—that jointly enable cross-task feature sharing and task-specific decoupling in a parameter-efficient manner.
- We demonstrate the effectiveness of our method on the *PASCAL-Context* benchmark, achieving superior multi-task performance compared to both fully fine-tuned and single-task PEFT baselines.

## 2 Related Works

**Learned Image Compression (LIC).** Learned Image Compression (LIC) was first introduced by Ballé et al. [4], which adopts an

autoencoder-based architecture to perform transform coding in the pixel space. Due to its superior rate-distortion (R-D) performance, LIC has shown great potential as a promising alternative to traditional image compression paradigms. A typical LIC codec consists of three key components: an analysis transform that maps the input image from the high-dimensional pixel space to a compact latent representation; an entropy model that encodes the latent variables into a compressed bitstream; and a synthesis transform that reconstructs the image from the latent space back to the pixel domain. The main research directions in LIC can be broadly categorized into two types. The first focuses on designing more efficient and expressive codec architectures, including more representative analysis and synthesis transforms. These structures have evolved from early CNN-based [4, 5, 9, 12, 33] designs to Transformer-based [23, 27, 31, 42] models, enabling better modeling capacity. In addition, recent efforts explore user-controllable compression, such as variable-rate coding [11, 22, 40] and distortion–perception [2] trade-off control, to enhance flexibility in practical applications. The second line of research focuses on designing more powerful entropy models to better estimate the probability distribution of latent representations. This has evolved from factorized [4] and hyperprior-based [5] models to more advanced autoregressive entropy models [18, 20, 21, 34–36]. However, most LIC methods are human-centric, as they are typically optimized using perceptual quality metrics such as MSE or LPIPS. While effective for human viewing, such objectives may not align with the needs of machine vision. In particular, pixel-wise distortion metrics tend to over-allocate bits to visually fine-grained details, while potentially neglecting semantically important structures that are critical for downstream vision tasks

**Image Compression for Machine Vision.** The rapid growth of computer vision applications has led to an increasing portion of visual data being consumed by machines rather than humans—for example, in autonomous driving, traffic monitoring, and visual surveillance. This shift motivates the need for image compression systems optimized for machine vision, aiming to jointly minimize transmission cost while preserving task-relevant information for downstream analysis. A straightforward solution is to define distinct encoder–decoder pairs tailored to each specific task. These approaches can be further categorized into two types: (1) Independent designs [6, 7, 17, 26], where each task is handled by a separately trained codec; and (2) Scalable designs [3, 15, 39], which share part of the model parameters while adapting to different tasks via task-specific components. However, this line of work often leads to multiple task-specific bitstreams and requires dedicated design for each task, resulting in increased system complexity and poor scalability as the number of tasks grows. An alternative line of work aims to extract a unified bitstream for multiple tasks. Specifically, these methods design a task-general encoder to produce semantically compact and generalizable representations that serve as a common source for all tasks. Task-specific outputs are then generated by applying either task-specific decoders [16, 25] or task-guided transformations [10] to adapt the shared representation to the needs of each downstream task. However, such codecs designed specifically for multiple vision tasks typically require non-trivial codec architecture design and computationally expensive training.

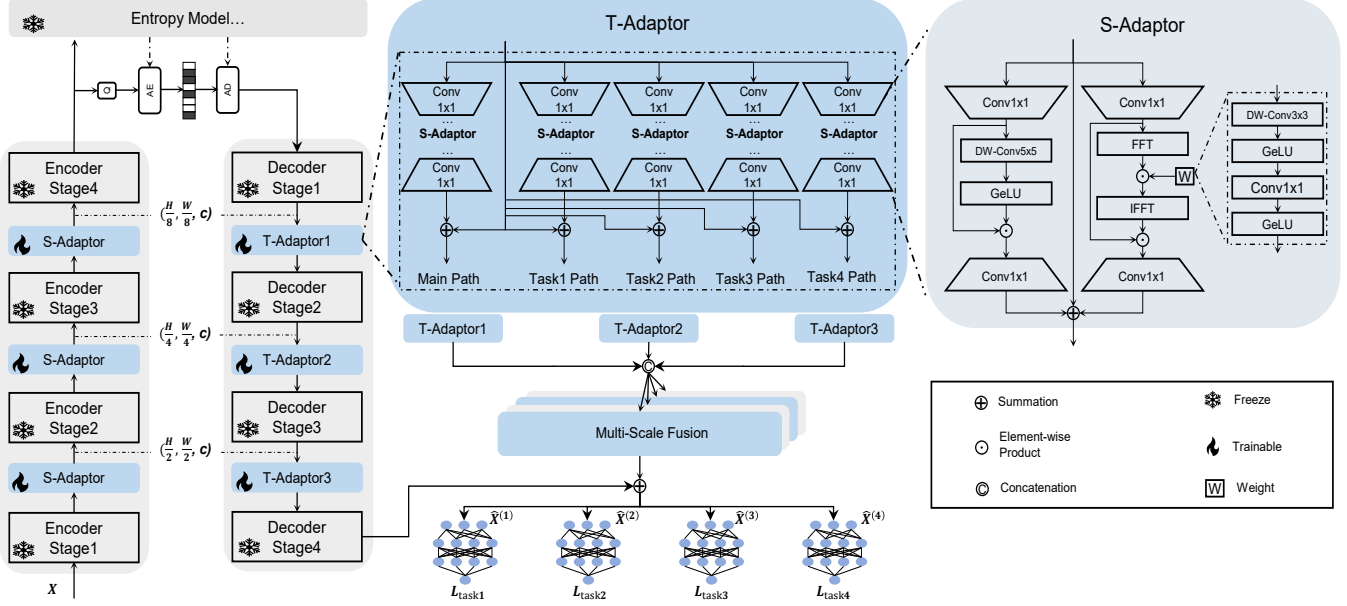


**Figure 2: Overview of our proposed architecture.** The backbone follows a typical autoencoder structure from *Lu2022-TIC*, consisting of an analysis network  $g_a$  and a synthesis network  $g_s$ . Each encoder and decoder stage includes a convolution layer to adjust feature resolution and a Residual Swin Transformer Block (RSTB) for enhanced representation learning. We introduce two types of adaptor modules: (1) Shared Adaptor (S-Adaptor) is inserted between encoder stages, with dual-branch modulating features in both spatial and frequency domains; (2) Task Adaptor (T-Adaptor) is inserted between decoder stages, composed of  $T$  task-specific paths (where  $T$  is the number of tasks), each independently processing task-specific features. T-Adaptor outputs are fed into task-specific feature aggregation modules for downstream processing.

making it difficult to scale to many tasks and challenging to deploy in practice.

**Transfer Human Perception to Machine Perception.** Most learned image compression (LIC) models are optimized for human perception, typically using distortion metrics such as MSE or LPIPS. Recent works have made progress by adopting tuning frameworks that transfer a pre-trained human-centric codec to various machine vision tasks. This pipeline enables ICMH (Image Compression for both Human and Machine) by training only a lightweight task-specific module while keeping the base codec frozen for shared use across human and machine perception. Unfortunately, these methods only support single-task optimization, requiring customized training for each task and producing separate bitstreams, which is not storage-efficient and leads to a linearly increasing training burden as the number of tasks scales up.

### 3 Method

**Problem Formulation.** Given a pre-trained base codec optimized for human perception, our goal is to efficiently transfer it to multiple machine vision tasks within a single unified model and through a single-stage training process. To achieve this, we adopt a multi-task adaptation framework that promotes feature sharing across tasks while preserving task-specific representations through structural decoupling, as illustrated in Figure 2. Furthermore, the training of our framework follows the parameter-efficient

fine-tuning (PEFT) paradigm by introducing lightweight plug-in modules, enabling effective adaptation without compromising the original rate-distortion performance of the base codec.

**Method Overview.** We begin in Section 3.1 by reviewing the base codec architecture and its human perception-based training objective. Then, in Section 3.2, we provide an overview of the key challenges in multi-vision transfer and introduce our asymmetric adaptor-based solution. Next, in Section 3.3, we detail the designs of the adaptation modules we employed, which enable efficient feature sharing and task-specific decoupling. Finally, Section 3.4 describes the joint optimization strategy used to train our model in an end-to-end manner.

#### 3.1 Preliminary

Learned Image Compression (LIC) frameworks typically adopt an autoencoder-based architecture, composed of an analysis network  $g_a$  and a synthesis network  $g_s$ . The encoder  $g_a$  maps the input image  $X$  from the high-dimensional pixel space to a more compact latent representation  $y$ , i.e.,  $y = g_a(X)$ . The decoder  $g_s$  then reconstructs the image from the quantized latent  $\hat{y}$ , i.e.,  $\hat{X} = g_s(\hat{y})$ . Naively storing the quantized latent  $\hat{y}$  can incur significant storage overhead. To address this, LIC models the distribution of symbols in  $\hat{y}$  via a learned entropy model  $p(\hat{y})$ , enabling efficient entropy coding. Throughout the compression process, the goal is to achieve a balance between compression rate and reconstruction quality. This

is formulated as an end-to-end optimization of the Rate-Distortion (R-D) trade-off:

$$\mathcal{L}_{rd} = \mathbb{E}_{X \sim p_X} [r(\hat{y}) + \lambda \cdot \mathcal{D}(X, \hat{X})] \quad (1)$$

where  $r(\hat{y})$  denotes the estimated bitrate,  $\mathcal{D}(X, \hat{X})$  is a distortion metric (e.g., MSE or LPIPS), and the hyperparameter  $\lambda$  controls the trade-off between compression rate and reconstruction quality.

In this work, we adopt *Lu2022-TIC* [31] as our base codec, which integrates convolutional layers and Transformer blocks in a hybrid architecture. This design enables the model to capture both local and long-range dependencies, supporting effective multi-scale feature extraction. Each encode and decode stage leverages a Residual Swin Transformer Block (RSTB) after a convolutional transformation, formulated as:

$$\mathbf{F}_i = \text{RSTB}(\text{Conv}(\mathbf{F}_{i-1})) \quad (2)$$

where  $\mathbf{F}_{i-1}$  is the input feature from the previous stage,  $\text{Conv}(\cdot)$  adjusts the spatial resolution, and RSTB captures contextual information through shifted window-based self-attention.

### 3.2 Framework Overview

Given a pre-trained image codec optimized for human perception (e.g., using MSE or LPIPS as the distortion metric), our goal is to adapt it efficiently to multiple downstream vision tasks within a single model. This poses a fundamental challenge: the model must strike a delicate balance between *feature sharing* and *task decoupling*. On one hand, different vision tasks often rely on partially overlapping visual cues (e.g., structural boundaries, semantic regions, textures), making shared representations beneficial. Effective feature sharing reduces redundancy, improves generalization, and helps prevent overfitting. On the other hand, excessive coupling may cause negative interference, such as easier tasks dominant more challenging ones. As a result, the architecture must support shared representation learning while preserving sufficient capacity for task-specific adaptation.

To address these challenges, we propose an asymmetric adaptor framework that extends the frozen base codec with two targeted architectural modifications, as illustrated in Figure 2 (Left). First, to enable generalizable feature extraction, we insert a *Shared Adaptor* (S-Adaptor) into each encode stage and the main path of the decode stage. The S-Adaptor adopts a dual-branch structure that captures both spatial and frequency-domain characteristics, serving as a task-agnostic feature pool for efficient representation sharing. Second, to support task-specific specialization, we insert a *Task Adaptor* (T-Adaptor) after each decode stage. The T-Adaptor comprises  $T$  parallel paths ( $T$  is the number of tasks)—one for each task, allowing each task to modulate shared features independently without mutual interference. Finally, the task-specific features from the T-Adaptor form a multi-scale hierarchy, where features at different resolutions encode information at varying levels. These are fused through a lightweight, task-specific aggregation module to generate residuals tailored for each task. The residuals are added to the shared reconstruction  $\hat{X}$  to produce the final task-specific output  $\hat{X}^{(t)}$  for downstream tasks.

### 3.3 Adaptation Modules

**S-Adaptor Design.** To promote feature generalization across tasks, we introduce the *Shared Adaptor* (S-Adaptor), a lightweight, task-agnostic modulation unit inserted into each encode stage as well as the shared main path of the decode stages. Besides learning shared representations, the S-Adaptor serves as an implicit communication hub, enabling inter-task interaction via a shared representation space without requiring explicit fusion operations.

Motivated by the observation that different vision tasks are sensitive to distinct frequency components [24], the S-Adaptor adopts a dual-branch architecture to extract both spatial and frequency-domain features. As illustrated in Figure 2 (Right), given an intermediate feature map  $\mathbf{F}_i^{\text{in}} \in \mathbb{R}^{H \times W \times C}$  from encode stage  $i$ , we apply spatial downsampling (omitted in the formulation for simplicity) to reduce computational overhead, followed by two parallel processing streams: (1) The spatial branch employs a depth-wise convolution to capture localized spatial patterns; (2) The frequency branch transforms the feature map into the frequency domain via 2D Fast Fourier Transform (FFT), modulates it with a learnable complex-valued mask  $\mathbf{M}_i$ , and reconstructs it via inverse FFT (IFFT). The outputs from both branches are fused as follows:

$$\mathbf{F}_i^{\text{out}} = \underbrace{\text{DWConv}(\mathbf{F}_i^{\text{in}})}_{\text{Spatial Branch}} + \underbrace{\text{IFFT}(\mathbf{M}_i \odot \text{FFT}(\mathbf{F}_i^{\text{in}}))}_{\text{Frequency Branch}} \quad (3)$$

Here,  $\text{DWConv}(\cdot)$  denotes depth-wise convolution, and  $\odot$  represents element-wise multiplication.  $\mathbf{M}_i$  is a learnable spectral mask that adaptively emphasizes or suppresses specific frequency components.

**T-Adaptor Design.** While the S-Adaptor supports shared representation learning, it lacks the ability to tailor features toward task-specific objectives. To address this limitation, we introduce the *Task Adaptor* (T-Adaptor), which performs task-specific modulation in a decoupled manner. As shown in Figure 2 (middle), the T-Adaptor is inserted after each decode stage and consists of  $T$  parallel paths—one per task. Each path follows the same dual-branch architecture as the S-Adaptor but is independently parameterized. Formally, the T-Adaptor at stage  $i$  is defined as:

$$\text{T-Adaptor}_i = \left\{ \text{T-Adaptor}_i^{(1)}, \text{T-Adaptor}_i^{(2)}, \dots, \text{T-Adaptor}_i^{(T)} \right\} \quad (4)$$

Given a shared feature  $\mathbf{G}_i \in \mathbb{R}^{H \times W \times C}$  from decode stage  $i$ , the modulated output for task  $t$  is computed as:

$$\mathbf{G}_i^{(t)} = \text{T-Adaptor}^{(t)}(\mathbf{G}_i), \quad t = 1, \dots, T \quad (5)$$

Here,  $\text{T-Adaptor}^{(t)}(\cdot)$  denotes the modulation path exclusively trained for task  $t$ , applied independently at each stage.

**Multi-scale Feature Fusion.** The task-specific features  $\mathbf{G}_i^{(t)}$  produced at different decode stages form a multi-scale representation hierarchy. To generate residual information tailored for each task, we aggregate these features using a lightweight multi-scale fusion module. The fused output is then added to the shared reconstruction  $\hat{X}$  to obtain the final task-specific prediction:

$$\hat{\mathbf{X}}^{(t)} = \hat{\mathbf{X}} + \text{Fuse} \left( \left\{ \mathbf{G}_i^{(t)} \right\}_{i=1}^3 \right), \quad t = 1, \dots, T \quad (6)$$

This design ensures that both low-level and high-level task-specific features are effectively integrated into the final reconstruction, enhancing task-adaptive detail refinement. The design of  $\text{Fuse}(\cdot)$  is discussed in detail in Section 4.5.

### 3.4 Optimization Strategy

Our framework is trained end-to-end to jointly optimize compression efficiency and downstream task performance. To quantify the compression efficiency, we adopt the rate-distortion formulation defined in Equation (1), which balances the trade-off between bitrate and reconstruction quality.

To incorporate supervision from downstream tasks, we define the task loss as a weighted combination of task-specific objectives:

$$\mathcal{L}_{\text{task}} = \sum_{i=1}^T w_i \cdot \mathcal{L}_i, \quad (7)$$

where  $\mathcal{L}_i$  is the loss for the  $i$ -th task and  $w_i$  controls its relative contribution.

The overall training objective combines both components:

$$\mathcal{L}_{\text{total}} = \lambda_{\text{rd}} \cdot \mathcal{L}_{\text{rd}} + \mathcal{L}_{\text{task}}, \quad (8)$$

where  $\lambda_{\text{rd}}$  balances the trade-off between compression and task performance. This formulation encourages the model to learn compact, bit-efficient representations that remain informative and effective for multiple downstream tasks.

## 4 Experiments

### 4.1 Experimental Setup

**Dataset.** We conduct our experimental evaluation on the PASCAL-VOC dataset [14], a widely-used benchmark in multi-task learning. Following prior works [1, 37, 41], we use the split of the PASCAL-Context subset with annotations for four vision tasks: *semantic segmentation*, *human parsing*, *surface normal estimation*, and *saliency detection*. The dataset contains 4,998 training images and 5,105 validation images. To meet codec constraints—which typically require image dimensions divisible by 64—all images are resized to 512×512 during both training and testing. In our experiments, we jointly optimize these four tasks within our single unified framework.

**Evaluation Metrics.** We use mean Intersection over Union (mIoU) to evaluate semantic segmentation, human part segmentation, and saliency prediction. For surface normal estimation, we report the root mean square error (RMSE) of the predicted angle differences. In addition, to assess the overall effectiveness of our multi-task learning, we adopt the *multi-task performance* metric  $\Delta m$  introduced in [32], which quantifies the average performance gain over its single-task counterparts. A higher  $\Delta m$  indicates better multi-task generalization.

$$\Delta m = \frac{1}{T} \sum_{i=1}^T (-1)^{l_i} (M_i - M_{\text{st},i}) / M_{\text{st},i} \quad (9)$$

where  $l_i = 1$  if lower is better for task  $i$ , and  $l_i = 0$  otherwise. Here,  $M_i$  and  $M_{\text{st},i}$  denote the performance of the multi-task and

single-task models, respectively. In our experiments, we use BD-acc as the task performance metric  $M_i$ . BD-acc is detailed in Section 4.3.

### 4.2 Implementation Details

**Our Framework.** Our framework is built upon the pre-trained *Lu2022-TIC* base codec, which remains frozen during training. Trainable parameters are introduced via two lightweight modules: the task-agnostic *Shared Adaptor (S-Adaptor)* and the task-specific *Task Adaptor (T-Adaptor)*. The S-Adaptor, shared across all tasks, is inserted into both encoder and decoder stages. In contrast, the T-Adaptor, placed only in the decoder stages, consists of four parallel paths corresponding to four downstream tasks. All S-Adaptors and T-Adaptor paths share the same architecture. The entire pipeline is trained end-to-end. Additionally, we analyze in the supplementary material how varying the reduction dimension within our adaptor modules impacts overall model performance.

**Baselines.** To benchmark our multi-task adaptation approach, we compare it with the following single-task tuning baselines: (1) **Full Fine-tuning**: All model parameters are fine-tuned independently for each task on top of the pre-trained base codec. (2) **Adaptor Tuning** [24]: Several trainable lightweight adaptor modules are inserted into each encoder and decoder stage of the base codec. (3) **Visual Prompt Tuning (VPT)** [8]: Trainable task-specific prompts are inserted into the transformer layers of the base codec.

All methods, including ours, are built upon the same base codec, *Lu2022-TIC*, and initialized with the pre-trained weights provided in [8] to ensure a fair comparison. For the Adaptor Tuning and Visual Prompt Tuning (VPT) baselines, we follow their official implementations and insert the PEFT modules into the encoder and decoder stages according to the configurations described in their respective papers.

**Training Setup.** All experiments are conducted using PyTorch on a single NVIDIA RTX 4090 GPU. All models are trained using the Adam optimizer with an initial learning rate of  $1 \times 10^{-4}$ . We apply a multi-step learning rate decay at epochs 2, 4, and 8 with a decay factor of 0.1. The total number of training epochs is set to 10.

We adopt the loss formulation described in Equation (8), combining rate-distortion loss and task objectives. For our method, task losses are balanced to a comparable scale following [37], and the weights remain fixed across all experiments. We vary the coefficient  $\lambda_{\text{rd}}$  within the range of 0.1 to 5.0 to explore the performance under different compression rates. The same strategy is applied to all baselines for fair comparison.

**Downstream Task Models.** For downstream task modeling, we adopted *MTLoRA* [1], which utilizes a Swin-Tiny [30] backbone coupled with a task-specific decoder head adapted from HRNet [38]. The model is pre-trained on ImageNet-1K [13] and then fine-tuned on multiple downstream tasks using LoRA [19].

### 4.3 Main Results

We compare our method against VPT, Adaptor Tuning, Full Fine-tuning, and the base codec (denoted as *TIC (Untuned)*). fig. 3 presents rate-accuracy curves, showing the performance of each baseline under varying compression rates. Meanwhile, Following prior work [8], we compute BD-rate and BD-accuracy to quantitatively measure

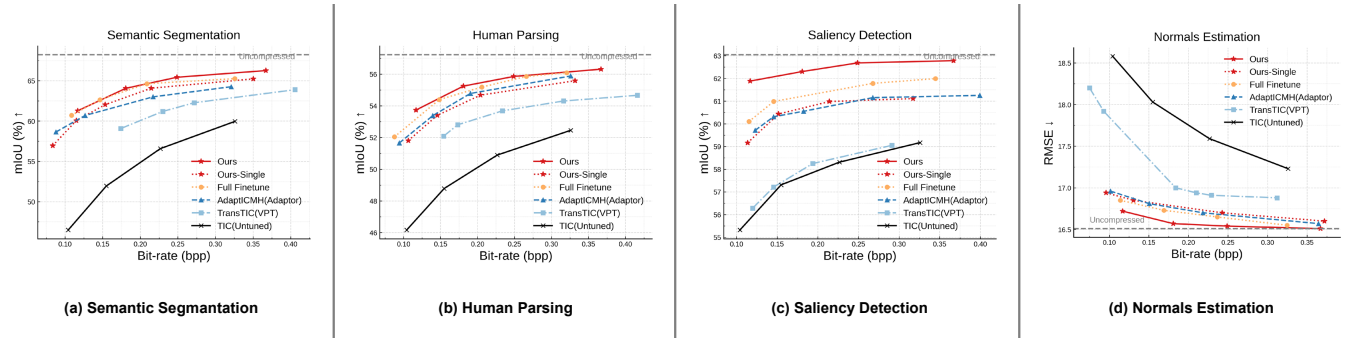


Figure 3: Rate-accuracy performance comparison across different machine vision tasks between our method and other baselines. We report our method uses a single bitstream compare to other baseline generating a separate bitstream per task.

Table 2: Comparison of rate-accuracy performance and trainable parameters (four tasks in total) across different tasks. BD-Rate and BD-Acc are computed with the base codec as anchor. Arrows indicate the preferred direction (↓: lower is better, ↑: higher is better). (–) indicates BD-Rate is not available.  $\Delta m$  denotes the performance gain of our multi-task model over single-task counterparts (higher is better), where we report BD-acc as the task metric. X indicates that multi-task learning is not supported.

Method	SemSeg		Human Parsing		Saliency		Normals		Trainable↓ Params (M)	Multi-Task / $\Delta m$ (%)
	BD-rate↓	BD-acc↑	BD-rate↓	BD-acc↑	BD-rate↓	BD-acc↑	BD-rate↓	BD-acc↑		
Full Fine-Tuning	-74.63%	9.63	-70.76%	5.23	-72.12%	3.53	-	1.09	30.04(100%)	X
TransTIC [8]	-39.99%	4.36	-49.16%	2.74	-6.00%	0.23	-56.47%	0.73	6.48(21.4%)	X
AdaptICMH [24]	-67.39%	8.45	-63.82%	4.78	-77.62%	2.76	-77.91%	1.09	1.15(3.7%)	X
Ours-Single Task	-63.24%	9.04	-61.61%	4.45	-64.37%	2.86	-80.36%	1.08	0.55 (1.8%)	-
<b>Ours</b>	<b>-74.89%</b>	<b>9.61</b>	<b>-78.91%</b>	<b>5.29</b>	<b>-</b>	<b>4.53</b>	<b>-</b>	<b>1.20</b>	<b>0.63 (2.1%)</b>	<b>+0.24</b>

performance in Table 2. BD-Rate calculate the average difference between two rate-distortion (RD) curves, indicating the bitrate savings at the same accuracy, while BD-acc compare the average accuracy difference between two rate-distortion (RD) curves, reflecting accuracy improvements at the same bitrate. For surface normal estimation (evaluated by RMSE, where lower is better), we negate the RMSE values before computing BD metrics.

We highlight the following experimental results:

(1) Across all four downstream tasks and under varying compression rates, our method consistently outperforms all baselines. This demonstrates the strong generalization and task adaptability of our method.

(2) Our approach is significantly more parameter-efficient, equiring only 2.1% of the trainable parameters of the base codec—just half the size of the adaptor-based baseline.

(3) our approach improve storage efficiency and deployment scalability. Unlike baselines that require training and storing a separate bitstream for each task, our method produces a single shared bitstream that serves all tasks.

(4) Our architecture demonstrates beneficial task interactions. Our multi-task model achieves better performance than its single-task counterparts, consistently across tasks and bitrates, as also reflected in the positive  $\Delta m$  score. This confirms the effectiveness of our multi-task architecture design.

#### 4.4 Qualitative Results

We visualize task-specific reconstruction results in Figure 4. Overall, our model allocates more bitrate to texture-rich regions as expected. And the preserved frequency components are adaptively tailored to the needs of each downstream task. Specifically, region-level semantic segmentation tasks emphasize spatial coherence, such as object boundaries, shapes, and consistent textures. As a result, the model tends to retain more mid- and low-frequency components. Human part segmentation, being even more semantically constrained, exhibits a stronger focus on low-frequency structures. In contrast, saliency detection aims to highlight visually distinctive regions, such as object edges, fine textures, and sharp intensity contrasts, which are typically characterized by high-frequency information. Therefore, reconstructions optimized for saliency retain more high-frequency details. Surface normals estimation, which predicts the per-pixel orientation of surfaces in 3D space, relies on both mid-frequency cues for smooth geometric transitions and certain high-frequency signals to capture fine-grained surface details. Consequently, its frequency distribution lies between that of segmentation and saliency tasks. We provide more visual reconstruction results in the supplementary materials.

#### 4.5 Ablation Study

**Multi-Scale Fusion Strategy.** Our T-Adaptors at different decoder stages generate multi-scale features that capture varying levels of information from the input image. Shallow-stage features,

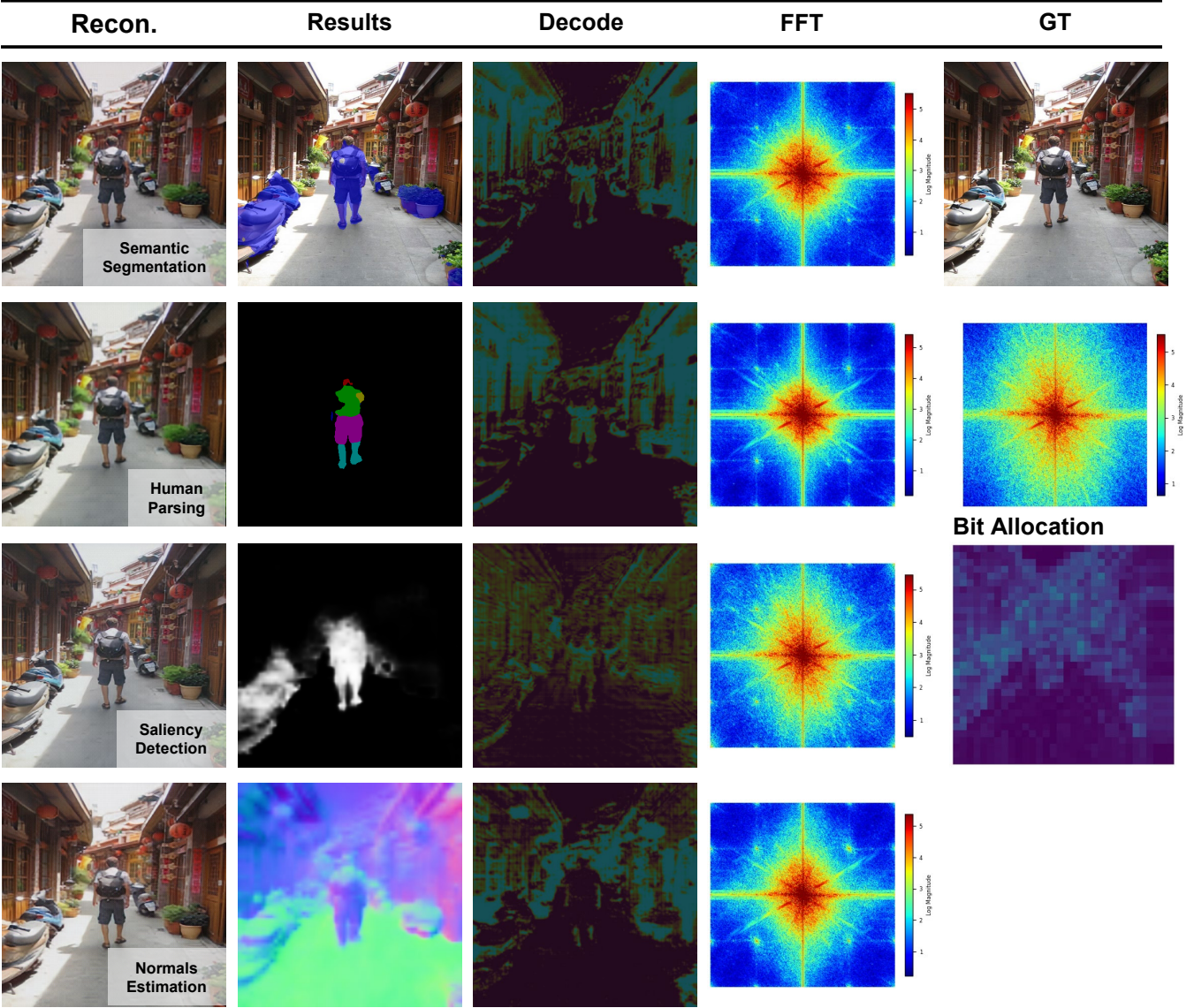


**Figure 4: Our Reconstruction results at 0.1168 bpp.** The first column shows reconstructions optimized for different vision tasks. The second column displays the corresponding downstream task predictions. The third column presents task-specific decoding output residuals, to better visualization, we generate residual heatmaps that highlight task-relevant differences. The fourth column visualizes the frequency-domain transformation of the reconstructed images. The fifth column includes the ground-truth images, corresponding frequency-domain representations, and the bit allocation maps after being compressed.

with smaller spatial resolutions, tend to represent higher-level semantics and geometric structures, while deeper-stage features capture finer details such as textures and edges. Although all scales are essential for accurate image reconstruction, they contribute differently to each downstream task. Effectively aggregating these multi-scale features is crucial for robust task performance. To this end, we compare three multi-scale fusion strategies, illustrated in Figure 6: (a) *Sum Fusion*: Features from different scales are spatially aligned and fused via element-wise summation. (b) *Cross-Scale Attention*:

Attention modules are applied across scales to adaptively weigh the importance of each feature map. (c) *Gate Fusion*: Learnable gates are used to control the contribution of each scale, enabling dynamic feature selection conditioned on task requirements.

We summarize the rate-accuracy comparison of different fusion strategies in Figure 5. Both Gate Fusion and Cross-Scale Attention achieve comparable and superior performance to Sum Fusion. Gate Fusion achieves slightly better results at lower bitrates, while Cross-Scale Attention excels under higher bitrates, which intuitively due

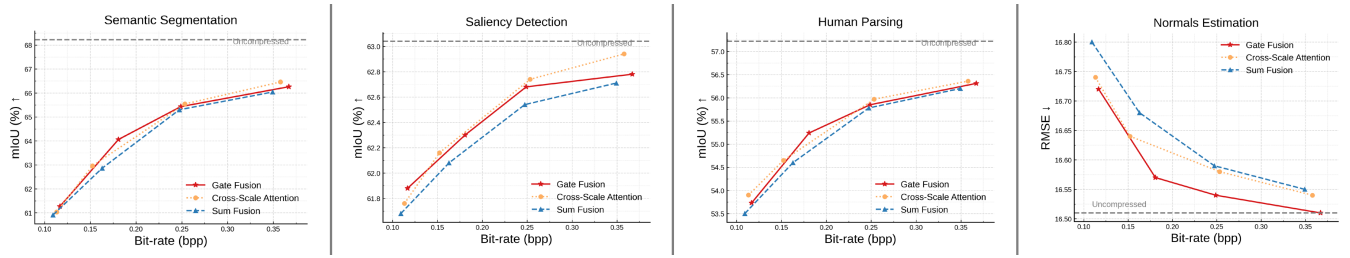


Figure 5: Comparison of multi-scale fusion strategies: (a) Sum Fusion, (b) Cross-Scale Attention, and (c) Gate Fusion.

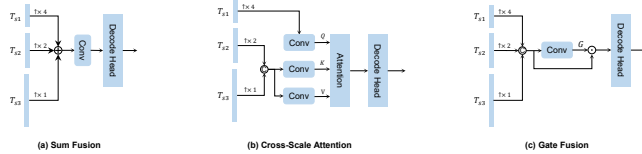


Figure 6: Comparison of multi-scale fusion strategies: (a) Sum Fusion, (b) Cross-Scale Attention, and (c) Gate Fusion.

Table 3: BD-rate and BD-acc Performance of Semantic Segmentation (SemSeg) and Human Parsing (Human) comparison under varying task number (set SemSeg as anchor task).

TASK (SemSeg)	SemSeg	Human Parsing
+Human	-69.82%/9.36	-71.01%/5.04
+Sal	-64.00%/9.33	-
+Human+Sal	-70.13%/9.39	-74.85%/5.22
+Human+Sal+Normals	-74.89% /9.61	-78.91%/5.29

to its global modeling capability benefiting from dense features. Considering the trade-off between performance, parameter count, and computational complexity, we adopt Gate Fusion in our main results reported in Figure 3 and Table 2.

**Task Number Scaling.** To further investigate the effect of task interaction and demonstrate the robustness of our method under task scaling scenarios, we evaluate its performance with varying numbers of downstream tasks. Specifically, we use semantic segmentation as the anchor task and incrementally add additional tasks to form four combinations: (1) +Human Parsing, (2) +Saliency Detection, (3) +Human Parsing + Saliency Detection, (4) +Human Parsing + Saliency Detection + Surface Normals.

We report both BD-rate and BD-acc for semantic segmentation and human parsing relative to the base codec, as summarized in Table 3. The results demonstrate that both tasks consistently benefit from multi-task interaction, with improved performance as more tasks are introduced. For a more intuitive comparison, we also provide the corresponding rate-accuracy curves in the supplementary material.

**Computation Complexity.** Although our method requires the fewest trainable parameters to adapt the base codec, the parallel

Table 4: Comparison of the kMACs/pixel and model size.

Method	Encoder	Decoder	Params (M)
TIC (Full-Finetune)	142.5	188.5	$7.51 \times 4$
TransTIC [8]	332.0	202.6	$1.62 \times 4$
AdaptICMH [24]	157.2	203.2	$0.29 \times 4$
<b>Ours</b>	149.7	236.1	$0.63 \times 1$

multi-path design of the Task Adaptors introduces additional architectural complexity, which may affect computational efficiency. To assess this impact, we follow prior works [8] and compare the complexity of competing methods using kilo multiply-accumulate operations per pixel (kMACs/pixel).

As shown in Table 4, inserting the single-path S-Adaptor into the encoder introduces the smallest increase in complexity among all PEFT baselines (from 142.5 to 149.7 kMACs/pixel). On the decoder side, the multi-path T-Adaptor introduces a higher increase in complexity, but within an acceptable range. It is also worth noting that Table 4 compares our multi-task setup against baselines in single-task settings. Overall, our method still demonstrates better computational efficiency than other competing approaches.

## 5 Conclusion

**Conclusion.** In conclusion, we introduce a novel asymmetric adaptation framework that enables efficient transfer of a human-centric base codec to a multi-task vision codec. Specifically, we design two lightweight plug-in modules: a task-agnostic *Shared Adaptor* for generalizable feature sharing, and a task-specific *Task Adaptor* for decoupled task modulation. The entire framework follows the PEFT training paradigm and requires only 2.1% of the trainable parameters to transfer to four downstream tasks, demonstrating its effectiveness under task number scaling.

Overall, this work offers a practical and effective solution for machine-centric image compression, and to the best of our knowledge, represents the first attempt at multi-task transfer in the codec transfer domain.

**Limitation.** As existing work on multi-task codec transfer remains scarce, we primarily compare our method against state-of-the-art single-task optimization baselines. While optimizing for a single task is inherently simpler than multi-task learning, and we conduct comprehensive evaluations of our approach under single-task, full multi-task, and partial task combination scenarios. Across

all settings, the results consistently validate the effectiveness of our proposed multi-task learning framework. We hope this work provides useful insights and encourages further research in the direction of multi-task codec transfer.

## References

- [1] Ahmed Agiza, Marina Neseem, and Sherief Reda. 2024. MTLoRA: A Low-Rank Adaptation Approach for Efficient Multi-Task Learning. arXiv:2403.20320 [cs.CV] <https://arxiv.org/abs/2403.20320>
- [2] Eirikur Agustsson, David Minnen, George Toderici, and Fabian Mentzer. 2023. Multi-Realism Image Compression with a Conditional Generator. arXiv:2212.13824 [cs.CV] <https://arxiv.org/abs/2212.13824>
- [3] Yuanchao Bai, Xu Yang, Xiaming Liu, Junjun Jiang, Yaowei Wang, Xiangyang Ji, and Wen Gao. 2021. Towards End-to-End Image Compression and Analysis with Transformers. arXiv:2112.09300 [cs.CV] <https://arxiv.org/abs/2112.09300>
- [4] Johannes Ballé, Valero Laparra, and Eero P. Simoncelli. 2017. End-to-end Optimized Image Compression. arXiv:1611.01704 [cs.CV] <https://arxiv.org/abs/1611.01704>
- [5] Johannes Ballé, David Minnen, Saurabh Singh, Sung Jin Hwang, and Nick Johnston. 2018. Variational image compression with a scale hyperprior. arXiv:1802.01436 [eess.IV] <https://arxiv.org/abs/1802.01436>
- [6] Lahiru D. Chamain, Fabien Racapé, Jean Bégaïnt, Akshay Pushparaja, and Simon Feltman. 2020. End-to-end optimized image compression for machines, a study. arXiv:2011.06409 [eess.IV] <https://arxiv.org/abs/2011.06409>
- [7] Lahiru D. Chamain, Fabien Racapé, Jean Bégaïnt, Akshay Pushparaja, and Simon Feltman. 2021. End-to-end optimized image compression for multiple machine tasks. arXiv:2103.04178 [cs.CV] <https://arxiv.org/abs/2103.04178>
- [8] Yi-Hsin Chen, Ying-Chieh Weng, Chia-Hao Kao, Cheng Chien, Wei-Chen Chiu, and Wen-Hsiao Peng. 2023. TransTIC: Transferring Transformer-based Image Compression from Human Perception to Machine Perception. arXiv:2306.05085 [eess.IV] <https://arxiv.org/abs/2306.05085>
- [9] Zhengxue Cheng, Heming Sun, Masaru Takeuchi, and Jiro Katto. 2020. Learned Image Compression With Discretized Gaussian Mixture Likelihoods and Attention Modules. arXiv:2001.01568 [eess.IV] <https://arxiv.org/abs/2001.01568>
- [10] Hyomin Choi and Ivan V. Bajic. 2022. Scalable Image Coding for Humans and Machines. *IEEE Transactions on Image Processing* 31 (2022), 2739–2754. doi:10.1109/tip.2022.3160602
- [11] Yoojin Choi, Mostafa El-Khamy, and Jungwon Lee. 2019. Variable rate deep image compression with a conditional autoencoder. In *Proceedings of the IEEE/CVF international conference on computer vision*. 3146–3154.
- [12] Ze Cui, Jing Wang, Shangyu Gao, Bo Bai, Tiansheng Guo, and Yihui Feng. 2022. Asymmetric Gained Deep Image Compression With Continuous Rate Adaptation. arXiv:2003.02012 [eess.IV] <https://arxiv.org/abs/2003.02012>
- [13] Jia Deng, Wei Dong, Richard Socher, Li-Jia Li, Kai Li, and Li Fei-Fei. 2009. Imagenet: A large-scale hierarchical image database. In *2009 IEEE conference on computer vision and pattern recognition*. Ieee, 248–255.
- [14] Mark Everingham, Luc Van Gool, Christopher KI Williams, John Winn, and Andrew Zisserman. 2010. The pascal visual object classes (voc) challenge. *International journal of computer vision* 88 (2010), 303–338.
- [15] Ruoyu Feng, Yixin Gao, Xin Jin, Runsen Feng, and Zhibo Chen. 2025. Semantically Structured Image Compression via Irregular Group-Based Decoupling. arXiv:2305.02586 [eess.IV] <https://arxiv.org/abs/2305.02586>
- [16] Ruoyu Feng, Xin Jin, Zongyu Guo, Runsen Feng, Yixin Gao, Tianyu He, Zhizheng Zhang, Simeng Sun, and Zhibo Chen. 2022. Image Coding for Machines with Omnipotent Feature Learning. arXiv:2207.01932 [cs.CV] <https://arxiv.org/abs/2207.01932>
- [17] Kristian Fischer, Fabian Brand, and André Kaup. 2024. Boosting Neural Image Compression for Machines Using Latent Space Masking. *IEEE Transactions on Circuits and Systems for Video Technology* (2024), 1–1. doi:10.1109/tcsvt.2022.3195322
- [18] Dailan He, Yaoyan Zheng, Baocheng Sun, Yan Wang, and Hongwei Qin. 2021. Checkerboard Context Model for Efficient Learned Image Compression. arXiv:2103.15306 [eess.IV] <https://arxiv.org/abs/2103.15306>
- [19] Edward J. Hu, Yelong Shen, Phillip Wallis, Zeyuan Allen-Zhu, Yuanzhi Li, Shean Wang, Lu Wang, and Weizhu Chen. 2021. LoRA: Low-Rank Adaptation of Large Language Models. arXiv:2106.09685 [cs.CL] <https://arxiv.org/abs/2106.09685>
- [20] Wei Jiang, Jiayu Yang, Yongqi Zhai, Peirong Ning, Feng Gao, and Ronggang Wang. 2023. MLIC: Multi-Reference Entropy Model for Learned Image Compression. In *Proceedings of the 31st ACM International Conference on Multimedia (MM '23)*. ACM, 7618–7627. doi:10.1145/3581783.3611694
- [21] Jooyoung Lee, Seunghyun Cho, and Seung-Kwon Beach. 2019. Context-adaptive Entropy Model for End-to-end Optimized Image Compression. arXiv:1809.10452 [eess.IV] <https://arxiv.org/abs/1809.10452>
- [22] Anqi Li, Feng Li, Yuxi Liu, Runmin Cong, Yao Zhao, and Huihui Bai. 2024. Once-for-All: Controllable Generative Image Compression with Dynamic Granularity Adaption. arXiv:2406.00758 [eess.IV] <https://arxiv.org/abs/2406.00758>
- [23] Han Li, Shaohui Li, Wenrui Dai, Chenglin Li, Junni Zou, and Hongkai Xiong. 2024. Frequency-Aware Transformer for Learned Image Compression. arXiv:2310.16387 [eess.IV] <https://arxiv.org/abs/2310.16387>
- [24] Han Li, Shaohui Li, Shuangrui Ding, Wenrui Dai, Maida Cao, Chenglin Li, Junni Zou, and Hongkai Xiong. 2024. Image Compression for Machine and Human Vision with Spatial-Frequency Adaptation. arXiv:2407.09853 [cs.CV] <https://arxiv.org/abs/2407.09853>
- [25] Jinming Liu, Ruoyu Feng, Yunpeng Qi, Qiuyu Chen, Zhibo Chen, Wenjun Zeng, and Xin Jin. 2024. Rate-Distortion-Cognition Controllable Versatile Neural Image Compression. arXiv:2407.11700 [cs.CV] <https://arxiv.org/abs/2407.11700>
- [26] Jinming Liu, Heming Sun, and Jiro Katto. 2022. Improving multiple machine vision tasks in the compressed domain. In *2022 26th International Conference on Pattern Recognition (ICPR)*. IEEE, 331–337.
- [27] Jinming Liu, Heming Sun, and Jiro Katto. 2023. Learned Image Compression with Mixed Transformer-CNN Architectures. arXiv:2303.14978 [eess.IV] <https://arxiv.org/abs/2303.14978>
- [28] Kang Liu, Dong Liu, Li Li, Ning Yan, and Houqiang Li. 2021. Semantics-to-signal scalable image compression with learned reversible representations. *International Journal of Computer Vision* 129, 9 (2021), 2605–2621.
- [29] Lei Liu, Zhihao Hu, Zhenghao Chen, and Dong Xu. 2023. Icmh-net: Neural image compression towards both machine vision and human vision. In *Proceedings of the 31st ACM International Conference on Multimedia*. 8047–8056.
- [30] Ze Liu, Yutong Lin, Yue Cao, Han Hu, Yixuan Wei, Zheng Zhang, Stephen Lin, and Baining Guo. 2021. Swin Transformer: Hierarchical Vision Transformer using Shifted Windows. arXiv:2103.14030 [cs.CV] <https://arxiv.org/abs/2103.14030>
- [31] Ming Lu, Peiyao Guo, Huiqing Shi, Chuntong Cao, and Zhan Ma. 2021. Transformer-based Image Compression. arXiv:2111.06707 [eess.IV] <https://arxiv.org/abs/2111.06707>
- [32] Kevis-Kokitsi Maninis, Ilija Radovovic, and Iasonas Kokkinos. 2019. Attentive Single-Tasking of Multiple Tasks. arXiv:1904.08918 [cs.CV] <https://arxiv.org/abs/1904.08918>
- [33] Fabian Mentzer, George Toderici, Michael Tschannen, and Eirikur Agustsson. 2020. High-Fidelity Generative Image Compression. arXiv:2006.09965 [eess.IV] <https://arxiv.org/abs/2006.09965>
- [34] David Minnen, Johannes Ballé, and George Toderici. 2018. Joint Autoregressive and Hierarchical Priors for Learned Image Compression. arXiv:1809.02736 [cs.CV] <https://arxiv.org/abs/1809.02736>
- [35] David Minnen and Saurabh Singh. 2020. Channel-wise Autoregressive Entropy Models for Learned Image Compression. arXiv:2007.08739 [eess.IV] <https://arxiv.org/abs/2007.08739>
- [36] Yichen Qian, Ming Lin, Xiuyu Sun, Zhiyu Tan, and Rong Jin. 2022. Entroformer: A Transformer-based Entropy Model for Learned Image Compression. arXiv:2202.05492 [eess.IV] <https://arxiv.org/abs/2202.05492>
- [37] Simon Vandenhende, Stamatios Georgoulis, and Luc Van Gool. 2020. MTI-Net: Multi-Scale Task Interaction Networks for Multi-Task Learning. arXiv:2001.06902 [cs.CV] <https://arxiv.org/abs/2001.06902>
- [38] Jingdong Wang, Ke Sun, Tianheng Cheng, Borui Jiang, Chaorui Deng, Yang Zhao, Dong Liu, Yadong Mu, Mingkui Tan, Xinggang Wang, Wenyu Liu, and Bin Xiao. 2020. Deep High-Resolution Representation Learning for Visual Recognition. arXiv:1908.07919 [cs.CV] <https://arxiv.org/abs/1908.07919>
- [39] Ning Yan, Changsheng Gao, Dong Liu, Houqiang Li, Li Li, and Feng Wu. 2021. SSSIC: semantics-to-signal scalable image coding with learned structural representations. *IEEE Transactions on Image Processing* 30 (2021), 8939–8954.
- [40] Fei Yang, Luis Herranz, Yongmei Cheng, and Mikhail G. Mozerov. 2022. Slimmable Compressive Autoencoders for Practical Neural Image Compression. arXiv:2103.15726 [eess.IV] <https://arxiv.org/abs/2103.15726>
- [41] Hanrong Ye and Dan Xu. 2022. InvPT: Inverted Pyramid Multi-task Transformer for Dense Scene Understanding. arXiv:2203.07997 [cs.CV] <https://arxiv.org/abs/2203.07997>
- [42] Renjie Zou, Chunfeng Song, and Zhaoxiang Zhang. 2022. The Devil Is in the Details: Window-based Attention for Image Compression. arXiv:2203.08450 [eess.IV] <https://arxiv.org/abs/2203.08450>